

Single-Chain Compaction of Long Duplex DNA by Cationic Nanoparticles: Modes of Interaction and Comparison with Chromatin

Anatoly A. Zinchenko,^{*,†,||} Takahiro Sakaue,^{‡,§} Sumiko Araki,[†] Kenichi Yoshikawa,^{†,||} and Damien Baigl^{*,§,||}

Department of Physics, Graduate School of Science, Kyoto University, Kyoto 606-8502, Japan, Yukawa Institute of Theoretical Physics, Kyoto University, Kyoto 606-8502, Japan, Department of Chemistry, Ecole Normale Supérieure, Paris F-75005, France, and Spatio-Temporal Order project, International Cooperative Research Project, Japan Science and Technology Agency, Japan

Received: November 29, 2006; In Final Form: January 12, 2007

The compaction of long duplex DNA by cationic nanoparticles (NP) used as a primary model of histone core particles has been investigated. We have systematically studied the effect of salt concentration, particle size, and particle charge by means of single-molecule observations—fluorescence microscopy (FM) and transmission electron microscopy (TEM)—and molecular dynamics (MD) simulations. We have found that the large-scale DNA compaction is progressive and proceeds through the formation of beads-on-a-string structures of various morphologies. The DNA adsorbed amount per particle depends weakly on NP concentration but increases significantly with an increase in particle size and is optimal at an intermediate salt concentration. Three different complexation mechanisms have been identified depending on the correlation between DNA and NPs in terms of geometry, chain rigidity, and electrostatic interactions: free DNA adsorption onto NP surface, DNA wrapping around NP, and NP collection on DNA chain.

Introduction

In eukaryotic cells, millimeter- to meter-long genomic DNA molecules are packaged into chromatin to fit within the micrometer-scale nucleic space. The elemental unit of chromatin is the nucleosome in which DNA wraps 1.7 times (147 base pairs) around an octamer of core histone proteins.¹ This octamer has an overall shape of a cylinder of 5 nm in height and 7 nm in diameter and carries approximately 220 positive electric charges.² Although genes are silent in higher-ordered structures such as the 30-nm chromatin fiber, genes are active in the open form of chromatin,^{3,4} which consists of nucleosomes distributed along a single duplex DNA chain and is usually referred to as a “beads-on-a-string” structure.^{5,6} Thus, long genomic DNA is naturally packaged in such a way that it is compacted at a very large scale while genes remain accessible.

On the other hand, long DNA molecules in a pure aqueous solution adopt an elongated coil state because of the electrostatic repulsion between negatively charged DNA monomers. In *in vitro* experiments, DNA molecules are thus usually compacted by the addition of a small amount of condensing agents,^{7,8} such as polyamines,⁹ multivalent metal cations,¹⁰ and cationic surfactants,¹¹ or in the presence of hydrophilic neutral polymers.¹² Such a change of the environment of DNA molecules induces a first-order phase transition at the level of single chains^{13,14} between the elongated coil state and a very dense compact state, or condensate, that is typically toroidal in shape and 100 nm in outer diameter.^{9,15} Consequently, when the length of DNA is

about 100 000 base pairs, there is no intermediate state between the coil and compact states and the monomer density is so large in the DNA condensates that transcription activity is completely inhibited and genes are constrained to silence.^{16,17}

Therefore, it seems to be essential to develop a new way of compacting long DNA molecules *in vitro* which would be closer to the natural packing of DNA by histone core proteins. This can be achieved by complexing genomic DNA to oppositely charged objects of nanosized dimensions and defined shape as in the chromatin of living cells.

The complexation of DNA with oppositely charged nanoparticles has been actively studied,¹⁸ but most frequently these studies dealt with “small” DNA molecules, that is, no longer than a few thousand base pairs (bp).^{19,20} Such complexes have a wide range of biotechnological applications¹⁸ as, for instance, transfection agents^{21–23} or biosensors.²⁴ As for the studies on longer DNA molecules, the thermodynamics of the interaction of calf thymus DNA (~10 000 bp) with nanometer-sized quantum dots has been studied by Mahtab et al.²⁵ Very long DNA molecules (>10 000 bp) have been mainly used as a scaffold for nanoparticles arrays²⁶ or as a template for metallic nanowires²⁷ or nanorings.²⁸ The interaction between DNA and soft oppositely charged complexing agents such as dendrimers has also been studied^{29,30} and is of practical interest for gene transfection.^{31,32} Keren et al.³³ characterized the microscopic structure of complexes composed of long DNA and positively charged complex at rather high concentration. Through these investigations, it has been getting clearer that the mode of interaction between semiflexible DNA chain and spherical polyions with sizes smaller than intrinsic DNA persistent length is strongly dependent on the correlation between DNA rigidity and size of nanosphere. By spectroscopic techniques, it was shown that an increase in size of spherical polycations changes the mechanism from the local assembly of polycations on the

* To whom correspondence should be addressed. E-mail: zinchenko@urban.env.nagoya-u.ac.jp, damien.baigl@ens.fr.

† Graduate School of Science, Kyoto University.

‡ Yukawa Institute of Theoretical Physics, Kyoto University.

§ Ecole Normale Supérieure.

|| Japan Science and Technology Agency.

DNA chain to the wrapping mechanism of DNA around the polycations. However, to our knowledge, the compaction of long, single-chain, double-stranded DNA by well-defined cationic nanoparticles as a model of histone core particles has never been investigated in detail up to now.

Inspired by biological significance of this system, many theoretical physicists have worked on the problem of semiflexible polyelectrolyte chain, such as DNA, interacting with oppositely charged spheres.^{34–40} Except for Monte Carlo simulations by Jonsson and Linse,⁴¹ most studies focused on the local interaction between a short segment of chain and one single oppositely charged sphere by neglecting the effect of the total DNA length or the number of particles per chain.

Also, there have been very few experimental reports on model systems in which long single-chain duplex DNA is compacted through the interaction with oppositely charged nanosized polycations.

Hence, we developed recently a series of cationic spherical polyions that can be used as a primary model of histone core proteins in the compaction of long duplex single-chain DNA.⁴² This system consists of well-defined monodisperse cationic nanoparticles (NP) with various sizes ranging from 10 to 100 nm and single-chain bacteriophage T4 DNA (57- μm contour length, 166 000 base pairs). The present article deals with a systematic detailed experimental investigation on the compaction of single-chain long T4 DNA by such histone-inspired cationic nanoparticles. By the combination of in-situ fluorescence microscopy (FM) observations in the bulk solution, transmission electron microscopy (TEM), and molecular dynamics simulations (MD), we analyzed the DNA/NP complexes at various stages of compaction. We studied the effect of salt concentration, particle size, and particle charge (preliminary study) on the overall DNA chain conformation and NP distribution, on the local organization of DNA on NP surface, on the amount of adsorbed DNA per NP, and on the mechanism of the DNA–NP interaction.

Materials and Methods

Materials. T4 DNA was purchased from Nippon Gene Co. Ltd., Japan. Silica nanoparticles were a gift from Nissan Chemical Industries Ltd., Tokyo, Japan (organosiloxasols IPA-ST, IPA-ST-MS, IPA-ST-L, and IPA-ST-ZL). Poly(L-lysine) ($M_w = 30\,000\text{--}70\,000\text{ g}\cdot\text{mol}^{-1}$), fluorescent dye DAPI (4'6-diamidino-2-phenylindole), spermine (*N,N'*-bis(3-amino-propyl)-1,4-diaminobutane), and NaCl were from Nacalai Tesque Inc. (Kyoto, Japan). Fluorescent dye Rhodamine Red-X was from Molecular Probes, Invitrogen (Tokyo, Japan). Deionized water (Milli-Q, Millipore) was used for all experiments.

Fluorescent Modification of Poly(L-lysine). Poly(L-lysine) at a concentration $10\text{ g}\cdot\text{L}^{-1}$ in water was labeled by Rhodamine Red-X fluorescent dye using a FluoReporter labeling kit (Molecular Probes) according to the procedure suggested by the manufacturer.

Nanoparticle Modification. Five microliters of a 30 wt % suspension of silica nanoparticles in isopropanol was first dispersed in 5 mL of pure water. This water suspension was then mixed with 3 mL of an aqueous solution of poly(L-lysine) at a total poly(L-lysine) concentration of $10\text{ g}\cdot\text{L}^{-1}$, containing 10 mol % of poly(L-lysine) labeled by Rhodamine Red-X. After 15 min of vigorous stirring, the poly(L-lysine)-modified particles were separated by centrifugation at 15 000 rpm for 90 min. The particles were then purified three times by addition of 15 mL of water followed by separation by centrifugation. Finally, nanoparticles were dispersed in water and were stored protected

from light at ambient temperature. Nanoparticles were used within two weeks after preparation.

Preparation of DNA/NP Complexes. For all experiments, we used T4 DNA solution at a concentration of $10^{-7}\text{ mol}\cdot\text{L}^{-1}$ (in nucleotides) in a $10^{-2}\text{ mol}\cdot\text{L}^{-1}$ Tris-HCl buffer solution (pH = 7.4). Nanoparticles were slowly added to the DNA solution under gentle stirring to prevent from DNA damage (chain breaking). The resulting DNA/NP complexes were observed 30 min after preparation.

Fluorescence Microscopy (FM). Sample solutions were prepared by successive mixing of water, Tris-HCl buffer solution ($10^{-2}\text{ mol}\cdot\text{L}^{-1}$), NaCl when needed (from 0 to $1.5\text{ mol}\cdot\text{L}^{-1}$), fluorescent dye DAPI ($10^{-7}\text{ mol}\cdot\text{L}^{-1}$), T4 DNA ($10^{-7}\text{ mol}\cdot\text{L}^{-1}$), and nanoparticles. Fluorescent microscopic observations were performed using an Axiovert 135 TV (Carl Zeiss, Germany) microscope equipped with a $100\times$ oil-immersed lens and selective filters for the fluorescence of DAPI (Abs/Em 350/420 nm) and Rhodamine Red-X (Abs/Em 570/590 nm), respectively. Fluorescent images were recorded using an EB-CCD camera and an image processor Argus 10 (Hamamatsu Photonics, Hamamatsu, Japan). Under these experimental conditions, we can directly observe the bulk conformation of a large number of individual DNA chains (DAPI filter) and localize simultaneously the actual position of individual nanoparticles (Rhodamine filter). Because of the blurring effect of fluorescence light, the apparent sizes of fluorescent images are approximately $0.3\text{ }\mu\text{m}$ larger than the actual sizes.

Transmission Electron Microscopy (TEM). Sample solutions for TEM were prepared in the same manner as for FM observations. TEM observations were performed at room temperature using a JEM-1200EX microscope (JEOL, Tokyo, Japan) at an acceleration voltage of 100 kV. We used carbon-coated grids with a mesh size 300. Each grid was placed for 3 min on top of a $15\text{-}\mu\text{L}$ droplet of DNA solution ($10^{-7}\text{ mol}\cdot\text{L}^{-1}$) on a Parafilm sheet. After the solution was blotted with filter paper, the grid was placed for 15 s on a $15\text{-}\mu\text{L}$ droplet of uranyl acetate (1% in water) for staining prior to final blotting and microscopic observation.

Molecular Dynamics (MD) Simulations. Numerical simulations of DNA/NP interaction were performed by using a coarse-grained model composed of a semiflexible polyelectrolyte and oppositely charged nanospheres. We prepared a polyelectrolyte chain modeled by N_m spherical monomers of diameter σ_m and charge z_m (in units of the elementary charge) and N_p spherical nanoparticles of diameter σ_p and charge z_p in a periodic cubic box of characteristic size $L = 100\sigma_m$. Adjoining monomers along the chain were connected by the harmonic bonding potential U_{bond}

$$U_{\text{bond}} = \frac{k_{\text{bond}}}{2\sigma_m^2} \sum_{\text{chain}} (|r_i - r_{i+1}| - \sigma_m)^2$$

where we chose a relatively large spring constant $k_{\text{bond}} = 400$ to keep the bond length at a nearly constant value σ_m . (Here and hereafter all energies are expressed in units of thermal energy $k_B T$). The mechanical stiffness of the chain is controlled by the following bending potential U_{bend}

$$U_{\text{bend}} = k_{\text{bend}} \sum_{\text{chain}} \left(1 - \frac{(r_i - r_{i-1})(r_{i+1} - r_i)}{\sigma_m^2} \right)^2$$

In the present study, we set the bending parameter $k_{\text{bend}} = 10$, which results in a mechanical persistence length $l_p = 12\sigma_m$.

All the particles and monomeric units interact through the electrostatic forces as well as the steric forces because of their excluded volumes (here modeled by the repulsive part of the Morse potential). As for the electrostatic part, we employed the linearized Debye–Hückel potential with the inclusion of the finite size effect of particles. The Debye–Hückel approximation is not quantitatively exact but is expected to produce qualitatively proper results. Therefore, the interaction between units I and J (here, I, J label either monomer or nanoparticle) separated by the distance r is

$$U_{IJ} = \frac{l_B z_i z_j}{(1 + \kappa \sigma_i/2)(1 + \kappa \sigma_j/2)} \frac{\exp[-\kappa(r - (\sigma_i + \sigma_j)/2)]}{r} + \exp[-\alpha(r - (\sigma_i + \sigma_j)/2)]$$

where l_B is the Bjerrum length ($l_B = e^2/(4\pi\epsilon k_B T) \approx 0.71$ nm in pure water at 298 K) and the inverse Debye screening length κ is tuned by the concentration of monovalent salt C_{salt} , that is,

$$\kappa = [4\pi l_B (2C_{\text{salt}} + (z_m N_m + z_p N_p)/L^3)]^{1/2} \approx (8\pi l_B C_{\text{salt}})^{1/2}$$

As for the exponent for the Morse potential, we adopted $\alpha = 24$, which ensured rather hard core repulsion.

The underdamped Langevin equation was employed for the time evolution (hydrodynamics interaction was neglected for simplicity). The equation of motion for i th units is governed by

$$m_i \frac{d^2 r_i}{dt^2} = -\gamma_i \frac{dr_i}{dt} + R_{i,i}(t) - \frac{\partial U}{\partial r_i}$$

where m_i , γ_i are the mass and friction constant of the monomer ($I = m$) or nanoparticle ($I = p$), respectively. Random force $R_{i,i}(t)$ is Gaussian white noise obeying the fluctuation–dissipation theorem. The internal energy U consisted of all the potential terms described above. The ratio of the friction constant between the core particle γ_p and the monomer γ_m was evaluated according to Stokes law. We chose a relatively large mass $m_m = m_p(\sigma_m/\sigma_p)^3 = 1$ to save calculation time, but all this setup associated with the inertial part should not affect the motion within the time scale of interest, which is much longer than the relaxation time of velocity. The dynamics of the system was performed using a leapfrog algorithm with a time step of $\Delta t = 0.005\tau$, where $\tau = \gamma_m \sigma_m^2/k_B T$ is a unit time step. Starting from random initial configurations, all simulations were carried out typically more than 10^5 time steps, which allowed us to obtain good statistics.

For the present study, we fixed monomer charge $z_m = -5$, Bjerrum length $l_B = 0.5 \sigma_m$, chain length $N_m = 200$, and varied Debye length κ^{-1} and parameters associated with nanoparticles: number N_p , size σ_p , and charge z_p .

Results and Discussion

Model Experimental System. We studied the interaction of individual long duplex DNA molecules with oppositely charged spherical particles of nanometer dimension (Figure 1a). As long DNA molecules, we used double-stranded T4 bacteriophage DNA (166 000 base pairs, 57- μ m contour length) at a concentration of 10^{-7} mol·L $^{-1}$ in nucleotides. At this concentration in a buffer solution (10^{-2} mol·L $^{-1}$ Tris-HCl in our study), individual T4 DNA molecules do not interact with each other and take an elongated coil conformation, because of monomer–monomer electrostatic repulsion, with large intrachain fluctuations because of thermal motion of monomers. Figure 1d shows

typical fluorescence microscopy (FM) images of T4 DNA molecule labeled by DAPI fluorescent dye. In this figure, an individual DNA molecule is observed as a fluctuating coil with a slow translational diffusive motion. On the other hand, cationic particles were prepared by the adsorption of Rhodamine-Red X labeled poly(L-lysine) onto silica nanoparticles of various sizes (Figure 1b, see Materials and Methods for details of the NP preparation). Four sets of nanoparticles have been prepared, namely, S, M, L, and XL, with mean diameters of ca. 10, 15, 40, and 100 nm, respectively. Figure 1c shows transmission electron microscopy (TEM) pictures of thus prepared cationic particles (i.e., after poly(L-lysine) modification) together with the size distribution established on ca. 100–200 specimens. The distribution of particle size is narrow regardless of particle size, and we have measured mean diameters of 10.7 ± 2.7 nm, 15.1 ± 3.6 nm, 41.7 ± 7.0 nm, and 99.3 ± 5.6 nm for S, M, L, and XL nanoparticles, respectively. By fluorescence microscopy of nanoparticles (Rhodamine-Red X fluorescence) in pure aqueous solution, particles appear as freely moving individual objects in solution with homogeneous Brownian diffusion coefficient (Figure 1e). This indicates that the nanoparticles are nearly monodisperse in diameter and are well dispersed in the aqueous medium (the presence of particle aggregates is negligible). From electrophoretic mobility measurements, the surface charge density of particles was estimated to be ca. $+1 \text{ e}\cdot\text{nm}^{-2}$ for all particles studied.

The interaction between individual DNA chains and nanoparticles was directly observed in the bulk solution by fluorescence microscopy, and the detailed morphology of the DNA/NP complexes was resolved by transmission electron microscopy. Furthermore, microscopic observations were complemented by molecular dynamics analysis of DNA–NP interaction.

In-Situ FM Observation of Single-Chain DNA Compaction. For in-situ observation of the DNA/NP interaction by fluorescence microscopy (FM), DNA and nanoparticles were labeled by two distinct fluorescent dyes. DNA was labeled by DAPI (Abs/Em 350/420 nm), while the nanoparticles were made fluorescent through preliminary modification of poly(L-lysine) with Rhodamine Red-X (Abs/Em 570/590 nm). Figure 2 shows the simultaneous FM observation of the specific fluorescence from DNA (Figure 2a) and nanoparticles (Figure 2b) and the schematic illustration of the observed interaction (Figure 2c) of single-chain DNA interacting with XL nanoparticles, as a function of an increasing concentration of nanoparticles. In the absence of nanoparticles ($[\text{NP}] = 0 \text{ wt } \%$), all individual DNA chains are in the typical elongated coil state characterized by a slow translational diffusion and large intrachain fluctuations (see also Figure 1d). When XL particles are added to the DNA solution ($[\text{NP}] = 2 \times 10^{-4} \text{ wt } \%$), one can observe that the DNA chain forms a complex with one nanoparticle (DNA/XL1). With a further increase in the XL concentration, the DNA chain forms successive complexes with two nanoparticles (DNA/XL2 at $[\text{NP}] = 4 \times 10^{-4} \text{ wt } \%$), three nanoparticles (DNA/XL3 at $[\text{NP}] = 6 \times 10^{-4} \text{ wt } \%$), and four nanoparticles (DNA/XL4 at $[\text{NP}] = 8 \times 10^{-4} \text{ wt } \%$), prior to full compaction ($[\text{NP}] = 1 \times 10^{-3} \text{ wt } \%$). Observed DAPI fluorescence is significantly brighter at the position of nanoparticles, indicating a higher local density of DNA around the nanoparticle, that is, a significant part of DNA chain is effectively adsorbed on each XL particle. Integration of DNA fluorescence intensity at the position of nanoparticles suggests that a similar amount of DNA is adsorbed on the different nanoparticles along the chain and for the successive steps of compaction. The process of the compaction

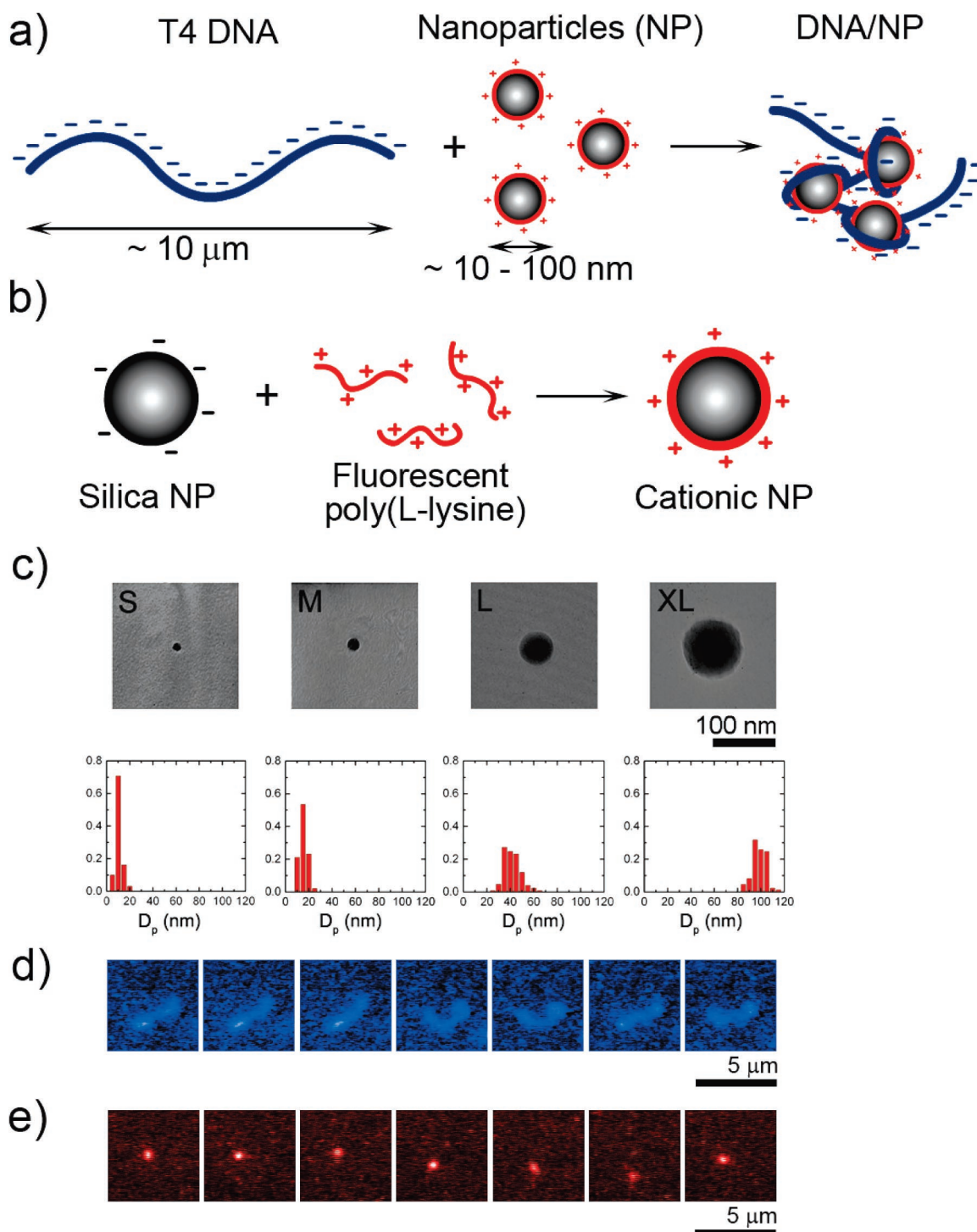


Figure 1. Experimental system. (a) As a model system, we used cationic nanoparticles (NP) of various sizes to compact single chains of long duplex DNA molecules (T4 DNA, 166 000 base pairs, contour length $57 \mu\text{m}$). We studied thus obtained DNA/NP complexes by means of fluorescence microscopy (FM), transmission electron microscopy (TEM), and molecular dynamics (MD) simulations. (b) Cationic NPs are formed by adsorption of fluorescent poly(L-lysine) onto silica nanoparticles (details in Materials and Methods). (c) TEM images (top) and size distribution (bottom) of the four sets of cationic NPs that have been prepared, namely, S, M, L, and XL, with mean diameters D_p of $10.7 \pm 2.7 \text{ nm}$, $15.1 \pm 3.6 \text{ nm}$, $41.7 \pm 7.0 \text{ nm}$, and $99.3 \pm 5.6 \text{ nm}$, respectively. (d) Time-dependent evolution of a single T4 DNA molecule ($10^{-7} \text{ mol}\cdot\text{L}^{-1}$ T4 DNA in $10^{-2} \text{ mol}\cdot\text{L}^{-1}$ Tris-HCl buffer) in the absence of NPs as observed by FM. Snapshots are separated by 0.2 s. (e) Time-dependent evolution of XL nanoparticle ($10^{-3} \text{ wt } \%$ in $10^{-2} \text{ mol}\cdot\text{L}^{-1}$ Tris-HCl buffer) in the absence of T4 DNA as observed by FM. Snapshots are separated by 0.2 s.

is gradual, in other words, the apparent size of the DNA chain decreases accompanied by the increase in the number of interacting XL nanoparticles per individual DNA chain. By observing a large number of individual DNA chains (approximately 200), we built the histograms of Figure 2d, which shows the fraction of each type of DNA/NP complexes (coil, DNA/XL1, DNA/XL2, DNA/XL3, DNA/XL4, and fully

compact) for the different NP concentrations. Inspection on the most probable state for each NP concentration indicates that the number of complexed nanoparticles per chain increases with an increase in the NP concentration. There is a majority of single-chain DNA complexed with one (at $[\text{NP}] = 2 \times 10^{-4} \text{ wt } \%$), then with two (at $[\text{NP}] = 4 \times 10^{-4} \text{ wt } \%$), with three (at $[\text{NP}] = 6 \times 10^{-4} \text{ wt } \%$), and with four particles

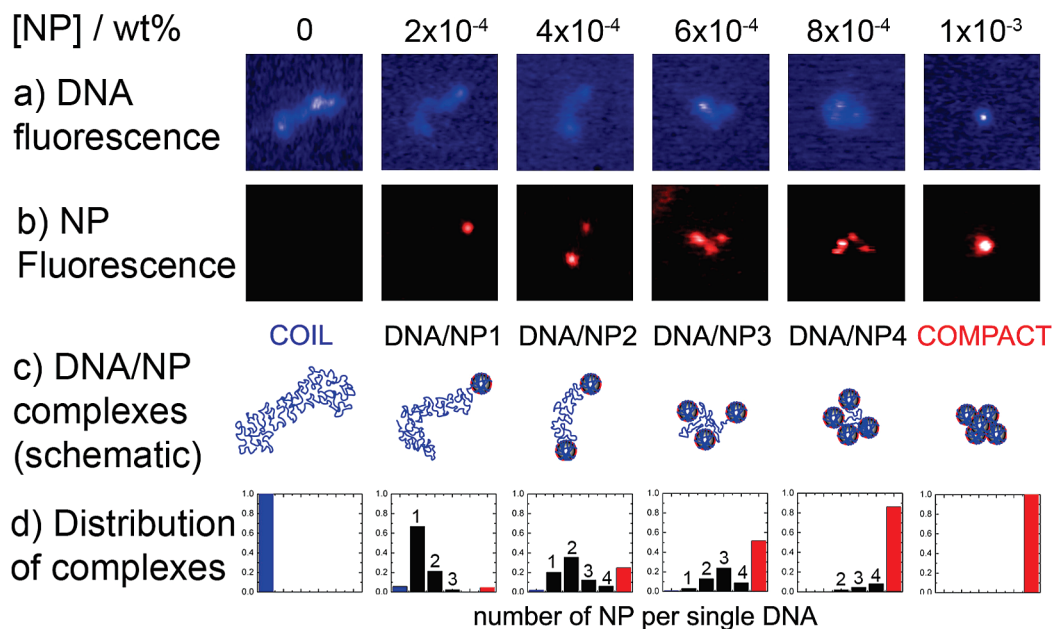


Figure 2. Fluorescence microscopy (FM) observations in the bulk solution of the interaction between a single DNA molecule (10^{-7} M) and nanoparticles (XL size) as a function of the nanoparticle concentration in Tris-HCl buffer solution (10^{-2} mol·L $^{-1}$). Each column corresponds to one nanoparticle concentration (from left to right: [NP] = 0, 2×10^{-4} , 4×10^{-4} , 6×10^{-4} , 8×10^{-4} , and 1×10^{-3} wt %). (a) Specific fluorescence emission of DAPI-labeled DNA. (b) Specific fluorescence image of Rhodamine-RedX labeled cationic nanoparticles. (c) Schematic representation of the DNA/NP complexes. From left to right: coil state; intermediate states, i.e., DNA/NP complexes with one (DN/XL1), two (DNA/XL2), three (DNA/XL3), and four (DNA/XL4) nanoparticles per DNA chain; and fully compact state. (d) Distribution of states—coil (blue bar), DNA/XL1 (1), DNA/XL2 (2), DNA/XL3 (3), DNA/XL4 (4), and fully compact state (red bar)—of individual DNA molecules for the successive NP concentrations.

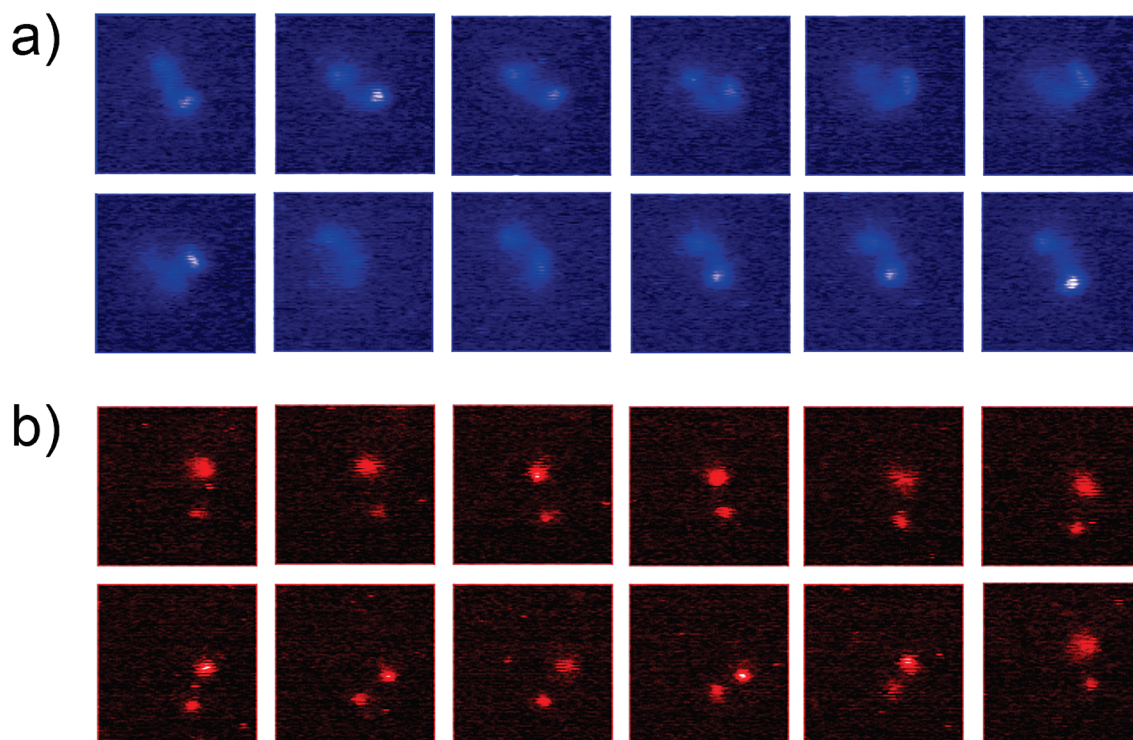


Figure 3. Time-dependent evolution of typical DNA/NP complexes for T4 DNA (10^{-7} mol·L $^{-1}$) in the presence of XL nanoparticles in Tris-HCl buffer solution (10^{-2} mol·L $^{-1}$). Fluorescence microscopy images of DNA/XL2 complex ([NP] = 4×10^{-4} wt %) (a) through DAPI filter selective for fluorescence from DNA and (b) through Rhodamine Red-X filter selective for fluorescence from NPs. For each series, snapshots are separated by 0.4 s.

(at [NP] = 8×10^{-4} wt %) while the fraction of DNA fully compacted by nanoparticles progressively increases with an increase in the NP concentration. At [NP] = 1×10^{-3} wt %, all DNA chains are in the fully compact state. The successive adsorption of DNA on particles induces the progressive shrinking of the chain, which is observed as a decrease in the long-axis length in the FM images (longest distance in the outline of

the DNA image), which is stepwise at the level of a DNA single chain. It may be obvious that, when the decrease in the long-axis length is averaged on a large ensemble of individual DNA chains, the transition appears as a continuous process.

Figure 3a and 3b shows the time evolution of a typical DNA/NP complex with 2 XL particles per chain. Through DAPI filter (fluorescence from DNA, Figure 3a), the DNA fluctuating

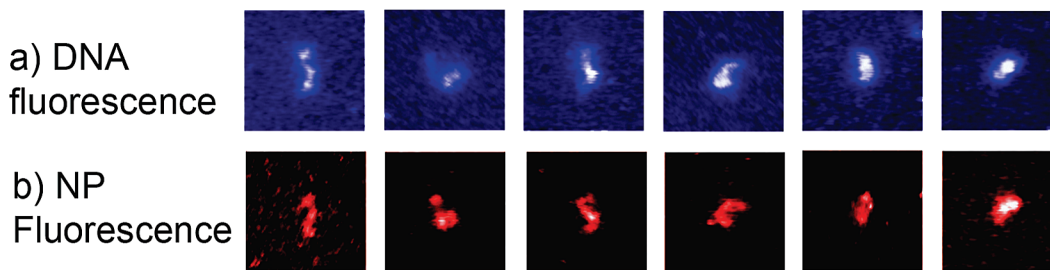


Figure 4. Fluorescence microscopy (FM) observation of the late stages of compaction of a single-chain DNA (10^{-7} mol·L $^{-1}$) by M nanoparticles in Tris-HCl buffer solution (10^{-2} mol·L $^{-1}$). Top: Specific fluorescence of DAPI-labeled DNA. Bottom: Specific fluorescence of Rhodamine Red-X labeled nanoparticles. NP concentration is 5×10^{-4} M (1–3) and 7×10^{-4} M (4–6) respectively.

coil part is seen connecting two parts on the chain with higher fluorescence intensity attributed to the DNA part adsorbed on the two XL nanoparticles. Then, when the same complex is observed through Rhodamine Red-X filter (fluorescence from NPs), one observes the correlated motion of the two XL nanoparticles complexed to the DNA chain. In contrast, the fully compact state appears as a bright, fast-diffusing spot without internal motion. In this case, it suggests that all the DNA chain has been adsorbed on the complexed nanoparticles, that is, the compaction has been fully achieved.

It is interesting to study the effect of particle size on the compaction phenomenology. Regardless of particle size, the whole process of compaction looks similar to that for XL particles described above in terms that single-chain DNA is progressively compacted when the nanoparticle concentration is increased and the DNA/NP complexes present typical intrachain fluctuations as long as DNA has not been fully compacted. The main differences are the number of intermediate states between the coil and the fully compact state and the apparent adsorbed DNA amount per particle. With a decrease in the particle size, the number of intermediate states and the maximum number of particles per chain increase significantly while the apparent amount of DNA per particle decreases. In the case of small nanoparticles (M and S), the number of NPs per chain in the late stages of compaction becomes so large that we cannot distinguish individual NPs on the DNA chain anymore. Figure 4 shows FM images of the late stages of compaction as a function of an increasing NP concentration. Through DAPI filter, one observes the shrinking of the DNA chain as the NP concentration is increased (Figure 4a). Simultaneous observations through Rhodamine Red-X filter show a diffusive fluorescence from NPs underlining the profile of the shrinking DNA chain with an increase in NP concentration (Figure 4b). With a decrease in NP size, the DNA adsorbed amount per particle decreases significantly. In this case, each new nanoparticle complexed to DNA in response to an increase in NP concentration is accompanied by a very small shrinking of the DNA chain, and the stepwise nature of the compaction becomes less pronounced.

All the above-mentioned experimental observations indicate that the DNA compaction by nanoparticles is stepwise and progressive at the level of the single chain, with several intermediate states that increase with a decrease in the particle size. The stepwise nature of the single-chain compaction becomes less pronounced with a decrease in the NP size. The intermediate states consist of parts of free, unfolded, single-chain DNA that connect particles on which a partial amount of DNA has been adsorbed. Regardless of the particle size, the number of particles per chain increases and the fraction of free, unfolded chain decreases when the nanoparticle concentration increases. Finally, with a further increase in NP concentration, the DNA chain is fully compacted. Full compaction corresponds

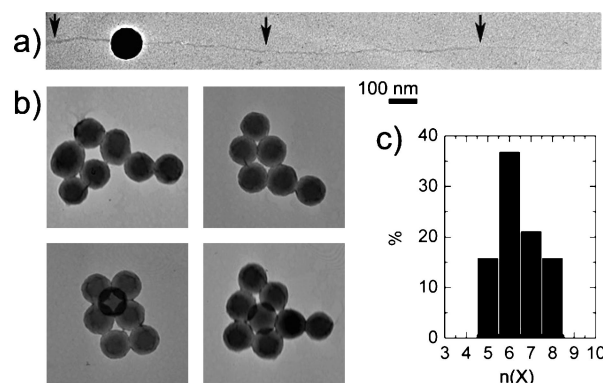


Figure 5. Transmission electron microscopy (TEM) observations of single-chain DNA (10^{-7} mol·L $^{-1}$) interaction with XL nanoparticles in Tris-HCl buffer solution (10^{-2} mol·L $^{-1}$). (a) Intermediate DNA–XL complex ([NP] = 5×10^{-4} wt %). (b) Final DNA–XL complexes ([NP] = 10^{-3} wt %). (c) Distribution of the number of XL nanoparticles per DNA fully compact state ([NP] = 10^{-3} wt %). About 50 DNA–XL complexes were analyzed. Images in a and b are shown at the same scale. Black arrows indicate parts of free, unfolded (not adsorbed) DNA chain.

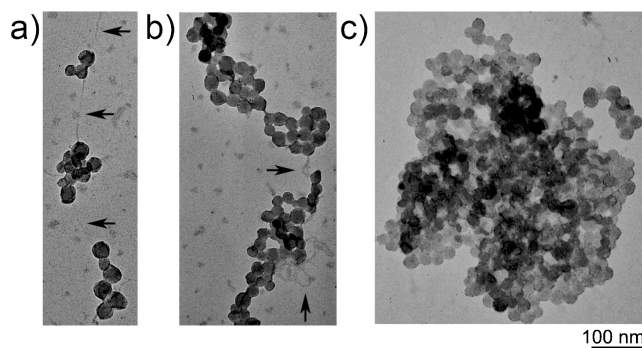


Figure 6. Transmission electron microscopy (TEM) images of single-chain DNA (10^{-7} mol·L $^{-1}$) complexes with M nanoparticles in Tris-HCl buffer solution (10^{-2} mol·L $^{-1}$). Nanoparticle concentration is (a) 5×10^{-4} wt %, (b) 7×10^{-4} wt %, and (c) 1×10^{-3} wt %. Images in a–c are shown at the same scale. Black arrows indicate parts of free, unfolded (not adsorbed) DNA chain.

to the disappearance of the free chain, all DNA being adsorbed on the complexed nanoparticles.

TEM Observation of DNA/NP Complexes: Intermediate and Fully Compact States. Transmission electron microscopy (TEM) was used to resolve the detailed structure of the DNA/NP complexes. Figures 5–8 show TEM images of the intermediate and fully compact states for different nanoparticle sizes. First, all intermediate DNA/NP complexes have a typical beads-on-a-string structure, which consists of nanoparticles connected by a thin thread (Figures 5a, 6a, and 6b). This linking thread is 2-nm wide and is assigned to free, unfolded, single-chain DNA (indicated by black arrows in Figures 5a, 6a, and 6b). The

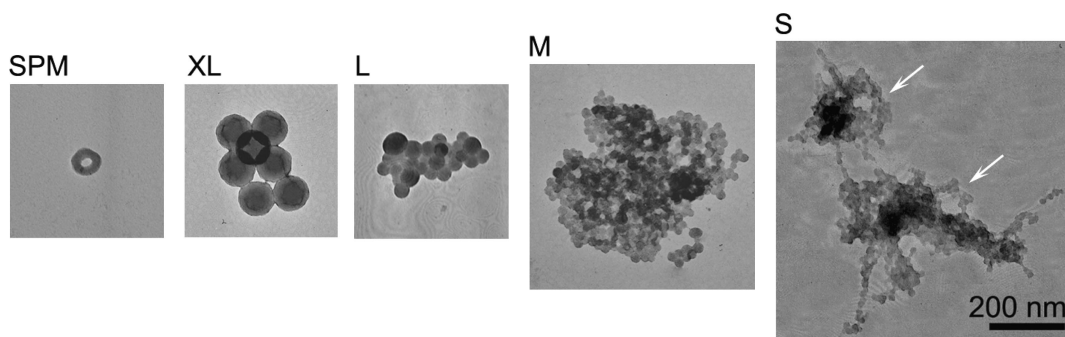


Figure 7. From left to right: Transmission electron microscopy (TEM) images of the fully compact state of single-chain DNA (10^{-7} mol·L $^{-1}$ in 10^{-2} mol·L $^{-1}$ Tris-HCl buffer solution) obtained in the presence of tetracation spermine SPM ([SPM] = 10^{-5} mol·L $^{-1}$), XL nanoparticles ([XL] = 10^{-3} wt %), L nanoparticles ([L] = 10^{-3} wt %), M nanoparticles ([M] = 10^{-3} wt %), and S nanoparticles ([S] = 10^{-2} wt %). White arrows indicate the formation of ring structure.

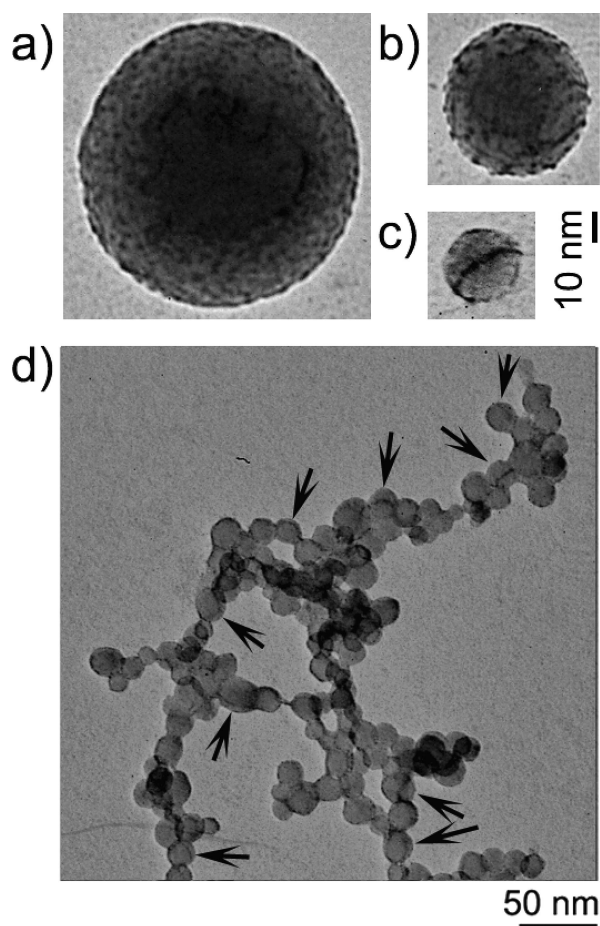


Figure 8. Transmission electron microscopy (TEM) images of the local arrangement of DNA chain on XL (a), L (b), and M (c and d) nanoparticles. T4 DNA concentration is 10^{-7} mol·L $^{-1}$ in 10^{-2} mol·L $^{-1}$ Tris-HCl buffer solution and NP concentration is (a) [XL] = 7×10^{-4} wt %, (b) [L] = 7×10^{-4} wt %, (c) [M] = 5×10^{-4} wt %, and (d) [M] = 5×10^{-4} wt %, respectively. Black arrows indicate nanoparticles onto which DNA wrapping is clearly visible.

presence of this free, unfolded DNA chain is responsible for the intrachain fluctuations of the DNA/NP complexes as observed by FM in the bulk solution (Figure 3a and 3b). Each bead corresponds to a nanoparticle onto which part of the DNA has been adsorbed. These beads-on-a-string structures present similarities with the structure of open chromatin, which consists of an array of nucleosome core particles, separated from each other by up to 80 base pairs of linker DNA.^{5,6,43,44} However, contrary to the periodic structure of natural open chromatin, nanoparticles are distributed in a nonperiodic way and can even

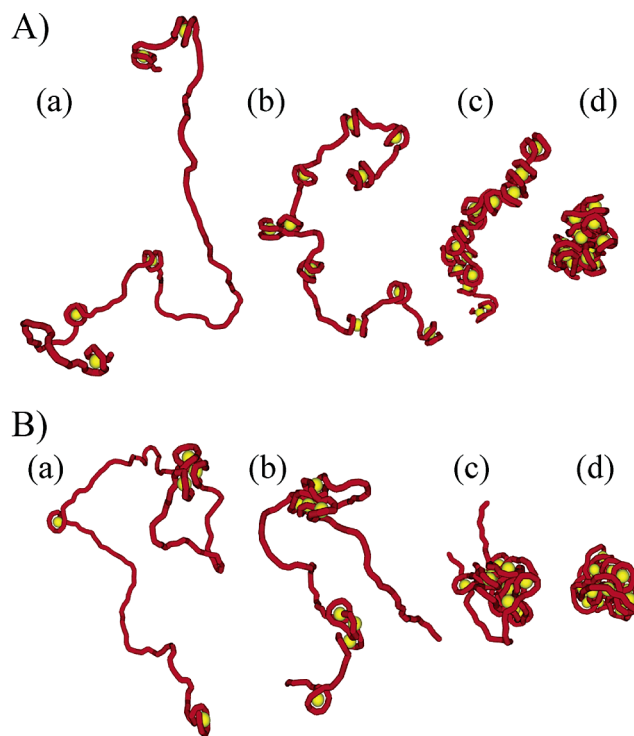


Figure 9. Typical snapshots obtained from molecular dynamics (MD) simulations on a semiflexible polyelectrolyte single-chain DNA in the presence of an increasing number of oppositely charged nanoparticles per DNA chain (a) $N_p = 5$, (b) $N_p = 10$, (c) $N_p = 15$, and (d) $N_p = 20$. For each series, the nanoparticle size σ_p was $2\sigma_m$ and the particle valency z_p was 40. The Debye length was fixed at (A) $\kappa^{-1} = 1\sigma_m$ and (B) $\kappa^{-1} = 0.3\sigma_m$, respectively. σ_m is the monomer diameter. The DNA chain is indicated in red and nanoparticles are indicated in yellow.

form small aggregates along the chain (Figure 6a). It is likely that the formation of aggregates is mediated by the DNA chain since such aggregates are not observed in the NP suspension without DNA (Figure 1c and 1e). The formation of segregated structures has been also observed in our MD simulations (see forthcoming section and Figure 9).

TEM observations of DNA complexation with the largest XL nanoparticles confirmed FM observations, that is, formation of DNA complexes with 1, 2, 3, and so forth nanoparticles when NP concentration is increased. In the case of intermediate states, these complexes consisted of 1–4 nanoparticles bound to a 2-nm-wide string, which is assigned to free single-chain DNA. For instance, Figure 5a shows a part of a DNA/XL complex where the free-single-chain DNA binding a nanoparticle is clearly identified (indicated by black arrows). With an increase in the NP concentration, the number of particles per chain

TABLE 1: Characteristics of Fully Compacted DNA–NP Complexes for XL, L, M, and S Nanoparticles^a

NP	NPs per chain	turns per NP
XL	5–8	23–36
L	40–50	9–11
M	600–1200	1–2
S	>5000	<0.3

^a Obtained from TEM observations: Number of nanoparticles NPs per DNA chain and corresponding average length of adsorbed DNA per nanoparticle expressed in terms of particle circumference or turns. Final DNA–NP complexes were analyzed in 0.01 mol·L⁻¹ Tris buffer solution at minimum NP concentration necessary for complete DNA compaction.

increases, while the fraction of free, unfolded chain decreases. This induces a progressive, overall shrinking of the chain as observed by fluorescence microscopy. With a further increase in NP concentration, DNA is finally fully compacted and a DNA–XL fully compacted state contains from 5 to 8 nanoparticles for one DNA chain (Figure 5b). Analysis of the number of XL nanoparticles per DNA chain in such a fully compacted state shows that the distribution is quite narrow and has a mean value of about 6 (Figure 5c). When the particle size decreases, the number of particles per chain increases significantly, indicating that a lesser amount of DNA is adsorbed on individual NP surface, which is in agreement with FM observations. The scenario of single-chain DNA compaction by smaller NPs is essentially the same as that by XL nanoparticles, except the increasing number of particles per chain. Figure 6 shows, for example, the compaction of single-chain DNA by M nanoparticles. At a low NP concentration, individual DNA molecule adsorbs on NPs available in the solution to form a beads-on-string structure where the nonadsorbed part of the chain connects individual or small groups of nanoparticles wrapped by adsorbed DNA (Figure 6a). With an increase in the NP concentration, the free part of DNA adsorbs on new particle inducing an overall shrinking of the chain together with an increasing number of particles per chain (Figure 6b). With a further increase in the NP concentration, DNA chain finally reaches the fully compact state in which the full length of the chain has been adsorbed on a quite large number of nanoparticles (Figure 6c). As mentioned before, complexed nanoparticles are not distributed in a periodic way on the DNA chain during the complexation process (intermediate states). When the NP size decreases, there is a tendency to clusterize upon complexation with DNA (e.g., Figure 6a), and this tendency becomes more pronounced when the number of nanoparticles per chain increases.

Finally, the number of particles per DNA chain in the final DNA–NP complex (fully compact state) is also strongly dependent on NP size. Figure 7 shows in the same scale a series of typical fully compact states, or condensates, of single-chain DNA as a function of the NP size. Although the path of individual DNA chain in these condensates cannot be fully traced, it is strongly suggested that these condensates contain one single DNA chain since most condensates for each sample observed by TEM have a similar size. Figure 7 suggests that the number of nanoparticles per DNA chain in fully compact state increases significantly with a decrease in the NP size. By analyzing a large number of condensates for each NP size, we have found that there are approximately from 5 to 8, from 40 to 50, from 600 to 1200, and more than 5000 NPs per fully compact state for XL, L, M, and S nanoparticles, respectively (Table 1). This corresponds well to the decrease of DNA adsorbed amount per particle with a decrease in NP size as mentioned before.

It is interesting to compare DNA/NP fully compact states obtained by interaction with cationic nanoparticles to DNA compacted by spermine, a tetracationic polyamine typically used as a DNA condensing agent. In the latter case, DNA charge neutralization induces the DNA folding, and a toroidal morphology with an outer diameter of 70–100 nm^{9,45} is adopted because of the native rigidity of the DNA double-stranded chain.^{46,47} For this purpose, Figure 7 shows at the same scale a series of TEM images of typical single-DNA fully compact states of T4 DNA in the presence of spermine or nanoparticles of various sizes. The comparison of DNA collapsed by multication and by nanoparticles makes clear the fact that DNA compacted by nanoparticles is distributed on nanosized subunits (the nanoparticles) and thus occupies an effective volume that is 5–10 times larger than that adopted by DNA upon self-assembly into a toroidal condensate. In our experimental conditions, single-chain DNA molecules compacted by spermine were about 70–90 nm in outer diameter while the overall size of DNA–NP compact states ranged from 300 to 600 nm for XL, L, and M particles with a weak dependence on particle size. The DNA–S complexes were slightly larger with a typical size of 600–800 nm. Moreover, since the amount of adsorbed DNA is almost independent of NP concentration, we may expect that the characteristic size of DNA–NP fully compact states decreases with a decrease in DNA contour length. In contrast, it is known that the size of DNA toroidal condensates compacted by a condensing agent such as spermine is mainly controlled by DNA rigidity and is almost independent of DNA contour length.

Arrangement of DNA Chain on Nanoparticle Surface. The arrangements of DNA on the surface of XL, L, and M nanoparticles in intermediate and final complexes are interesting to understand the DNA/NP interaction and mechanism of such interaction and to compare to the chromatin organization in which DNA wraps 1.7 times around every octamer of histone proteins. Typical examples of DNA chain arrangement on XL, L, and M nanoparticles are shown in Figure 8. In the case of large particles (XL, L), the part of DNA adsorbed on the particle is observed as a ribbed texture of the particle surface (Figure 8a and 8b). In controlled experiments without DNA, particle surface always appeared smooth and such texture has never been observed. Therefore, this ribbed texture is attributed to the presence of DNA and it suggests that a significantly important amount of DNA has been adsorbed on the particle surface, in agreement with the FM observations. For smaller particles, the amount of adsorbed DNA reaches the case when single-chain DNA makes one or a few turns around nanoparticle, and DNA chain can be clearly observed on the nanoparticle surface as a line with 2-nm width (this 2-nm line is attributed to DNA since it was never observed on NP surface in the absence of DNA or in the case of bare silica nanoparticles in the presence of DNA). Figure 8c shows a close-up of an M nanoparticle in a DNA/M complex ($[M] = 5 \times 10^{-4}$ wt %), where DNA chain makes clearly one turn around the nanoparticle. Figure 8d shows also a DNA/M complex but at a larger scale. In this complex, the DNA chain making one turn around individual particles is clearly observed on many particles of this complex (indicated by black arrows). There is almost one turn for every particle which confirms the assumption that adsorbed DNA amount per particle is nearly independent of particle concentration and stage of compaction. It is also consistent with the estimated amount of adsorbed DNA per NP as shown in Table 1. Moreover, DNA arrangement by wrapping the nanoparticles and making one turn around each NP is similar to DNA organization around histone core particle in the nucleosome. With a further decrease in

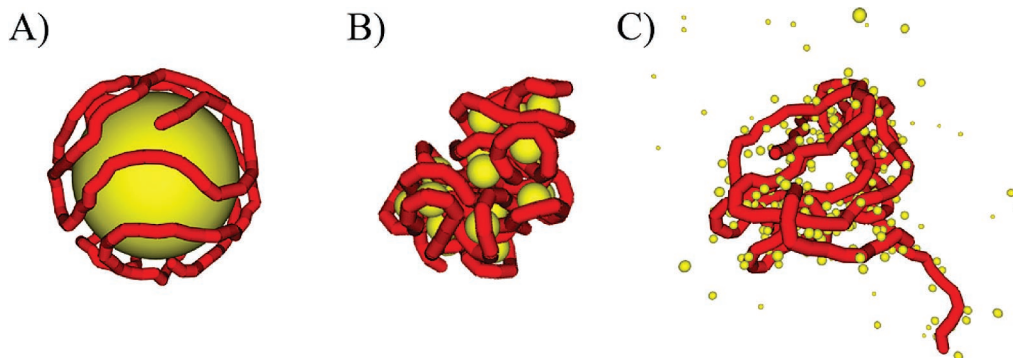


Figure 10. Typical snapshots obtained from molecular dynamics (MD) simulations of single-chain DNA fully compact state for (A) large, (B) medium, and (C) small nanoparticles. The diameter, valency, and number of nanoparticles are (A) $\sigma_p = 14 \sigma_m$, $z_p = 200$, $N_p = 1$; (B) $\sigma_p = 2\sigma_m$, $z_p = 40$, $N_p = 20$; and (C) $\sigma_p = 0.6\sigma_m$, $z_p = 4$, $N_p = 1000$. For each condition, the Debye length was fixed at $\kappa^{-1} = 1\sigma_m$. (σ_m is the monomer diameter). The DNA chain is indicated in red and nanoparticles are indicated in yellow.

nanoparticle size (S nanoparticles), we did not observe any DNA on nanoparticle surface, which shows that the wrapping of DNA around nanoparticle has become impossible. Instead, small nanoparticles are collected on the DNA charged surface as NP concentration is increased and the full compaction corresponds to the saturation of DNA chain by nanoparticles (Figure 7S). This collection mechanism is in agreement with a previously reported observation made on DNA interacting with cationic gold nanoparticles with a diameter of a few nanometers.^{26,48}

Special Case of Smallest Nanoparticles, “Ring” Motif in Final Condensates. Fully compact states of DNA with the smallest nanoparticles, which were formed by collection mechanism, have several special features. First, these complexes are significantly larger than complexes of DNA with larger size nanoparticles and they are observed as rather loose condensates of about 600–800 nm in overall size. Second, for this type of complex, we frequently observed a “ring” motif, which is indicated by a white arrow in Figure 7S. This motif is important and represents a special case of DNA chain behavior upon compaction by the smallest nanoparticles (S). This morphology was also observed in our MD simulations (see forthcoming section and Figure 10C). The ring shape is somewhat reminiscent of the toroidal morphology adopted by DNA chain compacted by low-molecular multications, such as spermine (Figure 7 SPM). It differs by the integration of NPs with a nanometric size within the compact structure.

Several scenarios can be proposed to explain the observed ring motif. For example, the loops are formed through complexation with NPs, which are not wrapped by DNA chain and stabilize the crossover contacts within the same DNA chain (kinetic effect). In the present case, we may suggest the following thermodynamic mechanism as a more plausible scenario. A dense toroidal structure with a high degree of orientational bond order is a consequence of the frustration between two competing factors: (1) strong and rather short-range effective attractive interaction between segments and (2) high rigidity of the DNA chain. However, in the case of the compaction by finite size nanoparticles, the effective range of the segment interaction would be longer, thus, the density of the collapsed state would be less than the usual dense toroid. This may lead to somewhat loose, nevertheless, locally ordered (because of the stiffness) structures. Such a mechanism was also confirmed in our MD simulations, where the DNA chain is observed to collect many small NPs to fold into a loose ringlike structure. (see forthcoming section and Figure 10C).

Estimation of the DNA Length Adsorbed per Particle. For a semiquantitative characterization of DNA/nanoparticle interaction, we estimated the amount of DNA adsorbed per particle

from microscopic observation. These simple calculations have been made on the basis of the average number of nanoparticles adsorbed on DNA chain and on geometrical parameters of system: length of adsorbed DNA (full length minus length of nonadsorbed free DNA chain) and average size of nanoparticle. At different stages of DNA compaction, the adsorbed amount of DNA per nanoparticle was weakly dependent on NP concentration but depended strongly on the particle size. Therefore, we used the average number of NP in the fully compact state and the full DNA contour length. Table 1 gives the number of nanoparticles per single-chain DNA condensate as determined by TEM for the different NP sizes. It shows that the number of particles per DNA fully compact state decreases significantly with an increase in the NP size, what corresponds to an increasing amount of DNA associated with a particle. The average adsorbed amount of DNA per particle was converted into an average DNA length adsorbed per particle and was expressed in terms of a number of turns (or NP circumference) per particle. The estimation of the number of DNA turns per adsorbed particle is also given in Table 1 for different particle sizes. It shows that there is a dramatic decrease in the amount of adsorbed DNA per particle with a decrease in the particle size. In the case of L and XL nanoparticles, the adsorbed amount of DNA per particle is quite large: 23–36 turns of DNA per NP and ~ 10 turns of DNA per NP for XL and L sizes, respectively. This important amount of DNA adsorbed on the NP surface is in qualitative agreement with the ribbed structures of the surface of those nanoparticles complexed by DNA as observed by TEM (Figure 8a and 8b). In the case of M nanoparticles, the adsorbed amount of DNA per NP decreases significantly with 1–2 turns of DNA on average per particle. These values correspond well to the DNA arrangement on NP revealed by our TEM experiments where the DNA chain was observed making one single turn around M nanoparticles (Figure 8c and 8d). Finally, in the case of the smallest nanoparticles (S), the adsorbed DNA length per NP is significantly smaller than one NP circumference. This confirms also our TEM experiments where the adsorption of nanoparticles onto the DNA chain is observed without DNA wrapping around individual nanoparticles. For additional verification of the amount of adsorbed DNA per particle, independent estimation of the DNA length adsorbed per nanoparticle was also made on the basis of AFM observations; it gave very similar values to that obtained from TEM and confirmed in particular the value of 1–2 turns of DNA per NP in the case of M nanoparticles (data not shown).

DNA/Nanoparticle Interaction as Studied by Molecular Dynamics (MD) Simulations. To gain deeper insight in the DNA/nanoparticle interaction mechanism, molecular dynamics

(MD) simulations have been performed on semiflexible charged chain (DNA) interacting with oppositely charged nanospheres of various sizes and at various NP concentrations and Debye screening lengths.

First, we studied the effect of NP concentration. Figure 9A and 9B shows a series of snapshots of the simulated DNA chain interacting with nanoparticles of a medium size ($\sigma_p = 2\sigma_m$; σ_m is the chain diameter) for an increasing NP concentration and for two Debye lengths (A) $\kappa^{-1} = 1 \sigma_m$ and (B) $\kappa^{-1} = 0.3 \sigma_m$. First, regardless of Debye length, it shows that the chain interacts strongly with the nanoparticles by adsorbing on the NP surfaces of opposite charge. The adsorption of DNA with nanoparticles is stepwise, that is, particles are complexed successively with an increase in the NP concentration. The adsorption of DNA on NP surface is accompanied by a decrease in the free (nonadsorbed) chain part and by a global shrinking of the chain. The fully compact state is reached when about 20 NPs have been complexed with the chain, which corresponds to a DNA/NP charge ratio of $200 \times 5/40 \times 20 = 1.25$. This confirms that NPs are overcharged by adsorbed DNA. There is also a clear tendency for DNA to wrap around the nanoparticles, which confirms the TEM observations on DNA complexed with M particles (Figure 8c and 8d). Finally, it can be noticed that nanoparticles are not distributed periodically on the chain but in a random way and may form clusters depending on the conditions. In fact, Figure 9 shows that the decrease in the Debye screening length is accompanied by a more globular conformation of the DNA/NP complex (e.g., $N_p = 15$) and a more pronounced tendency for clusterization (e.g., $N_p = 5$ and $N_p = 10$). Such a partially collapsed structure appears to be analogous to the intrachain segregation observed in charged polymers under collapsing transition, such as hydrophobic polyelectrolytes^{49,50} or giant DNA folding transition.^{51–53} Also, all DNA/NP complexes obtained in our simulations, except for fully collapsed ones, are fluctuating structures with a rich dynamic behavior.⁵⁴ All these results are in very good agreement with the single-chain observations by fluorescence and electron microscopy.

Estimation of the amount of adsorbed DNA (Table 1) on the NP surface and electron microscopy observations (Figures 7 and 8) suggest a strong influence of particle size on the DNA/NP interaction. For further understanding of the effect of NP size, we performed MD simulations where the semiflexible polyelectrolyte chain interacts with oppositely charged nanospheres of various sizes. We added nanoparticles step by step in the simulation box until the DNA reached the fully compact states (no apparent free chain). Figure 10 shows the DNA/NP fully compact states for three NP sizes: very large ($\sigma_p = 14\sigma_m$), medium size ($\sigma_p = 2\sigma_m$), and very small ($\sigma_p = 0.6\sigma_m$). For a very large NP size, the chain adsorbs almost flat and erratically on the NP surface (Figure 10A), nearly as a polyelectrolyte on an oppositely charged flat surface.⁵⁵ This can be understood since the mechanical persistence length $l_p = 12\sigma_m$ is smaller than the NP diameter. For a medium NP size, for example, $\sigma_p = 2\sigma_m$, chain stiffness and monomer–monomer electrostatic repulsion of the polyelectrolyte chain becomes significantly important in the adsorption process of the polyelectrolyte onto individual nanoparticles. In this case, our simulations showed that the chain tends to wrap around nanoparticles by adsorbing nearly parallel and making almost two turns around each complexed nanoparticle. This can be observed in the fully compact state (Figure 10B) as well as at every stage of compaction (Figure 9A, a–d), in good agreement with our TEM observation (Figure 8c and 8d, approximately

one turn per particle under corresponding experimental conditions). This spontaneous organization of a long semiflexible polyelectrolyte chain around nanoparticles is remarkably similar to the DNA wrapping around histone core particles in the nucleosome, in which many specific and local interactions between DNA and core proteins are also included.²

In the case of very small nanoparticles, the DNA/NP interaction changes drastically. In the early stages of compaction, the small nanoparticles adsorb on the DNA chain with very few changes in the overall extension and shape of the DNA chain. A very large number of nanoparticles is necessary to induce compaction of the DNA chain. When the number of nanoparticles introduced in the simulation box is high enough, for instance, about 1000 for one DNA chain in the case of a nanoparticle with a diameter $\sigma_p = 0.6\sigma_m$, the DNA/NP complex tends to fold into compact structures. Under the present condition, the collapsed structures are typically loose and are characterized by a local orientational order, which possibly results in a structure with a hole (Figure 10C). This is in qualitatively good agreement with the emergence of ring motifs in the DNA/S fully compact states observed by TEM (Figure 7S). As mentioned before, such a loose structure would be the consequence of the “loose” profile of the effective intersegment interactions. Therefore, it is expected that denser and more ordered toroidal structures are formed by tuning system parameters, such as a coupling of the electrostatic force, the Debye length, and the chain stiffness.

Three Modes of DNA Chain Interaction with Nanoparticles. Microscopic observations of DNA/NP complexes, MD simulations of DNA/NP interaction, and nanostructural arrangement of DNA chain on nanoparticles with different sizes suggest three distinct cases of DNA/nanoparticles complexation: adsorption, wrapping, and collection.

In the case of large XL and L nanoparticles, DNA chain adsorbs randomly on nanoparticle surface. For infinitely large particles, this adsorption would be a two-dimensional adsorption of DNA chain on the charged surface as on a planar oppositely charged surface.⁵⁵ This way of complexation is characterized by a very large amount of adsorbed DNA per particle and a small number of particles complexed with a single DNA chain. We will refer to it as an “adsorption” mechanism. When the size of NP is significantly smaller than DNA persistence length (M nanoparticles), DNA rigidity becomes significantly important and complexation is realized by a single turn or by a few turns of DNA chain wrapping parallel (like a solenoid) around individual nanospheres. We thus qualify this way of DNA/NP interaction as a “wrapping” mechanism. Actually, this wrapping mechanism can be considered as a particular case of adsorption mechanism; however, it might possess some unique features as possibility of NP slipping along DNA chain.^{56,57} Moreover, the regular arrangement of DNA around the nanoparticles can be important for precise sequence recognition or positioning. Finally, in the extreme case of very small S nanoparticles, even single wrapping is not realized because of the high-energy cost to wrap a small nanoscale object. In this case, the small nanoparticles adsorb on the DNA chain surface; the number of NPs necessary to fully load a long DNA chain, such as genomic T4 DNA, is extremely large. We refer to this way of DNA/NP interaction as a collection mechanism.

The existence of three mechanisms of interaction—adsorption, wrapping, and collection—depending on the nanoparticle size is in good agreement with the Monte Carlo simulations of Chodanowski and Stoll.⁵⁸ Experimentally, flexible polyelectrolytes (PE) are known to adsorb easily even on very small

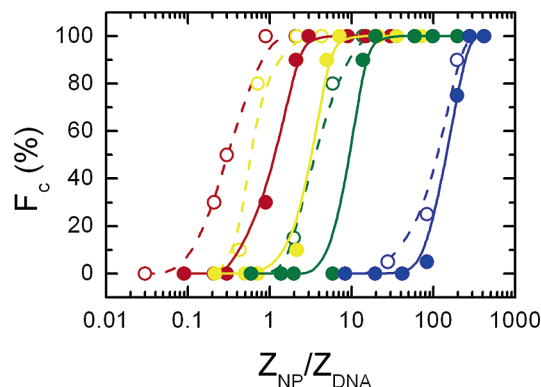


Figure 11. Compaction curves. Percentage F_c of DNA chains in the fully compact state as a function of the charge ratio (Z_{NP}/Z_{DNA}) of the total charge of nanoparticles to the total charge of DNA for XL (red), L (yellow), M (green), and S (blue) nanoparticles. Compaction curves have been established on the observation of approximately 200 individual DNA chains, in $10^{-2} \text{ mol}\cdot\text{L}^{-1}$ Tris-HCl buffer solution (pH = 7.4), without added salt (solid symbols and solid lines) and in the presence of $10^{-2} \text{ mol}\cdot\text{L}^{-1}$ NaCl (open symbols, dashed lines).

nanoscale polycations⁵⁹ while rigid PE usually collect even large nanoparticles. The semiflexible nature of DNA favors the occurrence of the three mechanisms of interaction—adsorption, wrapping, and collection—in a practically accessible range of particle sizes (1–100 nm).

Microscopic observations and MD simulations of DNA in the presence of cationic nanoparticles made clear the existence of three distinguished modes of interaction between DNA chain and cationic nanoparticles. For further quantitative analysis, DNA compaction by nanoparticles under different conditions was analyzed by systematic fluorescent microscopy observations.

Effect of Particle Size and Salt Concentration. To study systematically the effect of particle size and salt concentration, we monitored DNA/NP interaction by building compaction curves, that is, the percentage of DNA molecules in the fully compact state as a function of the NP concentration, for various experimental conditions (salt concentration, particle size, and particle charge). Each compaction curve was obtained by measuring the fraction F_c (%) of DNA molecules in a fully compact state among approximately 200 individual molecules. Figure 11 shows compaction curves obtained for different sizes of nanoparticles at two total salt concentrations. Zero fraction of compact DNA indicates that at the particular concentration of NP no fully compacted DNA chains were observed but intermediate DNA/NP complexes might be present. Since the NP charge concentration is not a linear function of NP size, NP weight concentration was converted into an dimensional charge ratio Z_{NP}/Z_{DNA} obtained by dividing the total charge brought by nanoparticles Z_{NP} (using NP concentration and NP charge density from ζ -potential measurements) by negative charge of all DNA molecules Z_{DNA} . Compaction curves are thus plotted as a function of Z_{NP}/Z_{DNA} ratio.

Figure 11 shows the compaction profiles of DNA with XL, L, M, and S nanoparticles in $10^{-2} \text{ mol}\cdot\text{L}^{-1}$ Tris-HCl buffer solution and after addition of NaCl ($10^{-1} \text{ mol}\cdot\text{L}^{-1}$). It indicates that, regardless of NP size and addition of salt, DNA chains are compacted with an increase in NP concentration and that, when NP concentration is large enough, all DNA molecules are finally fully compacted ($F_c = 100\%$). It shows also that, with a decrease in NP size, the Z_{NP}/Z_{DNA} charge ratio necessary to compact all DNA chains increases dramatically. For instance, by comparing XL and S nanoparticles, the difference in the

positive charge, which is necessary to compact DNA completely, differs over 2 orders of magnitude. This evolution correlates well with the different mechanism of interaction: adsorption for large nanoparticles (XL, L), wrapping for medium size nanoparticles (M), and collection for smallest nanoparticles (S). Furthermore, it is interesting to study the effect of added salt on compaction efficiency. Regardless of particle size, the charge necessary to compact all DNA chains decreases significantly with the addition of salt, and this effect is particularly pronounced for small particles (S, M), that is, under conditions of collection or wrapping mechanism.

To further elucidate the effect of salt on DNA/NP interaction, we performed the following systematic experiments. The NP concentration was fixed and NaCl concentration was varied before adding DNA. For each NaCl concentration, we analyzed the fraction of DNA chain in compact state in a similar manner as for Figure 11. Figure 12 shows the fraction of DNA chains in the fully compact state as a function of total salt concentration C_s ($10^{-2} \text{ mol}\cdot\text{L}^{-1}$ buffer solution + NaCl at various concentrations) for different NP sizes. First, regardless of NP size, the overall effect of total salt concentration is similar: (1) at a low salt concentration, the compaction efficiency increases with an increase in C_s , (2) the compaction efficiency is optimal at an intermediate salt concentration, and (3) with a further increase in C_s , a strong decrease in compaction efficiency is observed. This overall salt effect on compaction efficiency by cationic nanoparticles is markedly similar to that reported for natural histones, that is, salt-induced complexation under low salt conditions⁶⁰ and salt-induced release under high-salt conditions.⁶¹ Moreover, the optimum of compaction activity by NPs corresponds to a total salt concentration of about $0.1 \text{ mol}\cdot\text{L}^{-1}$, regardless of NP size. This value corresponds well to typical physiological salt concentrations at which the optimal complexation is also achieved in the case of histone proteins.

The existence of such an optimum can be explained as a consequence of interplays between attractive and repulsive electrostatic interactions involved in the system. First, at a low salt concentration, DNA stiffness is higher because of the long-range monomer–monomer electrostatic repulsion (electrostatic persistent length).^{62–64} This change in DNA persistent length l_p as a function of κ^{-1} has been confirmed experimentally; for instance, l_p was measured to decrease from $60 \pm 5 \text{ nm}$ at $C_s = 0.01 \text{ mol}\cdot\text{L}^{-1}$ to $48 \pm 2 \text{ nm}$ at $C_s = 0.1 \text{ mol}\cdot\text{L}^{-1}$ ^{65,66} and should affect the wrapping of DNA around NPs. In particular, the wrapping–unwrapping transition is expected for the case of M particles. Second, since the complex should possess some negative residual charge at the onset of the compaction (overcharging of NPs by DNA), the electrostatic self-energy of the compacted complex increases at lower salt concentrations. Both these factors arising from the increase in Debye length κ^{-1} make the compact state unfavorable at lower salt concentrations. In contrast, under high salt conditions, the Debye length becomes so small that the DNA nanoparticle electrostatic attraction becomes screened out and the DNA adsorbed amount decreases markedly with an increase in C_s , which corresponds well to the decrease in F_c observed in Figure 12. Mainly driven by DNA local rigidity and electrostatic interactions, the general profile—increase, plateau, decrease of F_c as a function of C_s —is observed for all the particle sizes studied. This common behavior shows that the existence of an optimal salt concentration for the efficiency of oppositely charged nanoparticles to compact semiflexible DNA is a universal phenomenon, which is not restricted to the specific case of DNA/histone interaction. Moreover, although this general tendency is the same regardless

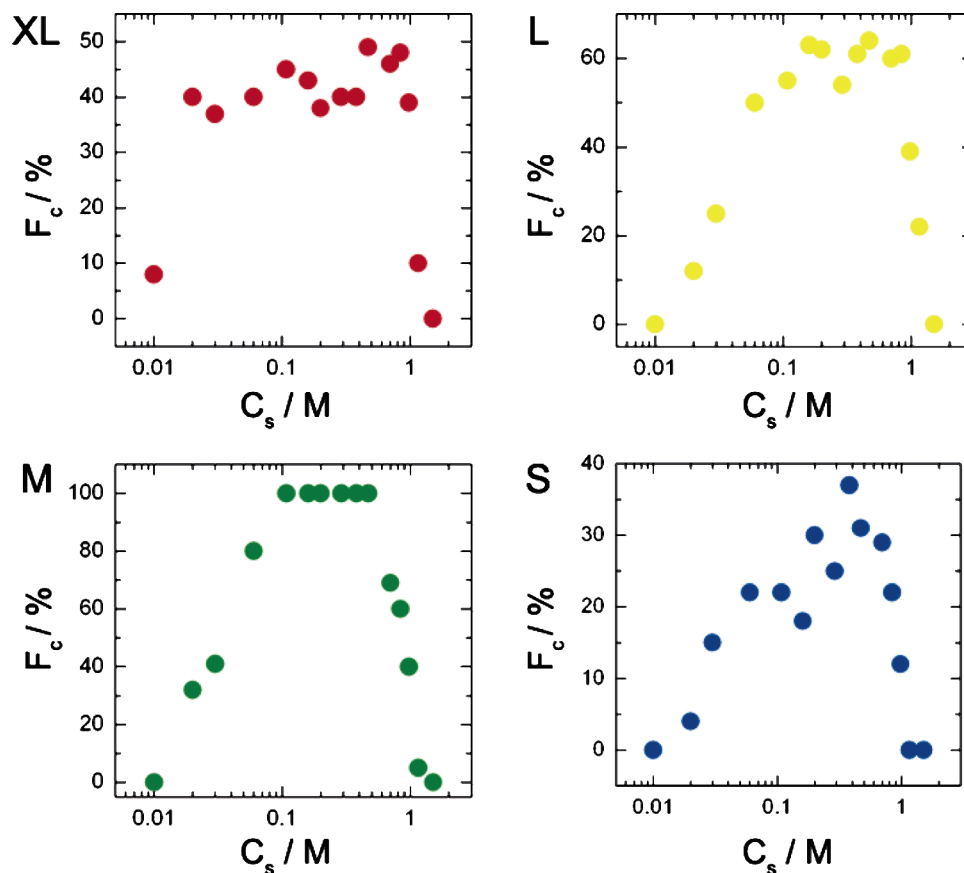


Figure 12. Percentage F_c of DNA chains in the fully compact state as a function of the total salt concentration C_s for XL (upper left, red symbols), L (upper right, yellow symbols), M (lower left, green symbols), and S (lower right, blue symbols) nanoparticles. The nanoparticle concentration was fixed as follows: $[XL] = 10^{-4}$ wt %, $[L] = 10^{-4}$ wt %, $[M] = 7 \times 10^{-4}$ wt %, and $[S] = 10^{-3}$ wt %, respectively.

of NP size, NP size has an influence on the shape of the evolution. Indeed, Figure 12 shows that the slopes of the salt-induced complexation under low salt conditions, and of the salt-induced decomplexation under high-salt conditions, decrease markedly with a decrease in NP size. This evolution is accompanied by a marked decrease in the width of the plateau region of F_c versus C_s . The plateau region corresponds to the situation where the amount of adsorbed DNA per nanoparticle is maximum and independent of salt concentration. We may expect that with a decrease in NP size, wrapping DNA around nanoparticles becomes more sensitive to salt concentration because of the electrostatic cost of bending DNA. Finally, in the limited case of very small nanoparticles (S), the increase of salt concentration can induce a transition between a collection configuration (low DNA adsorption) and a wrapping mechanism (high adsorption) under low salt conditions and a reverse transition from wrapping to collection and eventually to release of nanoparticles under high salt conditions.

Conclusion and Perspectives

In this article, we have reported on the single-chain compaction of long duplex DNA by cationic nanoparticles (NPs) used as a primary model of histone core particles. By using a unique combination of single-chain experiments, fluorescence microscopy observations, TEM characterization, and MD simulations, we have grasped the systematic influence of NP size, and total salt concentration on DNA/NP interaction upon DNA compaction. We have found that DNA compaction is progressive, stepwise at the single-chain level, and proceeds through the formation of beads-on-a-string structures of various morphologies. The amount of DNA adsorbed per particle is nearly

independent of NP concentration but increases significantly with an increase in particle size and charge and is optimal at an intermediate salt concentration. Three different adsorption mechanisms have been identified depending on the correlation between DNA and NPs in terms of geometry, chain rigidity, and electrostatic interactions: free DNA adsorption onto NP surface, DNA wrapping around NP, and NP collection on DNA chain. Our investigations revealed many features similar to DNA/histone interaction: beads-on-a-string formation, DNA wrapping mechanism, and optimal complexation under physiological conditions. Nevertheless, new features specific to DNA/NP interactions have been unveiled: adsorption and collection mechanism, irregular beads-on-a-string structures, and formation of kinetically trapped states. The latter point is now under investigation by preparing DNA/NP complex with a dialysis method similar to that typically used for reconstitution of chromatin. Finally, further studies on model systems containing long DNA chain and cationic nanoparticles will shed light upon capability of such systems to be used for biological or biotechnological applications.⁶⁷

Acknowledgment. This work was supported by the grants No. P03200, No. P04154, and No. 01263 from the Japanese Society for the Promotion of Science (JSPS). This work is partly supported by Grant-in-Aid for Scientific Research No. 18719001 from MEXT, Japan.

References and Notes

- (1) Kornberg, R. D. *Science* **1974**, *184*, 868–871.
- (2) Luger, K.; Mäder, A. W.; Richmond, K. R.; Sargent, D. F.; Richmond, T. J. *Nature* **1997**, *38*, 251–260.

- (3) Dorigo, B.; Schalch, T.; Kylangara, A.; Duda, S.; Schroeder, R. R.; Richmond, T. J. *Science* **2004**, *306*, 1571–1573.
- (4) Francis, N. J.; Kingston, R. E.; Woodcock, C. L. *Science* **2004**, *306*, 1574–1577.
- (5) Olins, A. L.; Olins, D. E. *Science* **1974**, *183*, 330–332.
- (6) Thoma, F.; Koller, T.; Klug, A. *J. Cell. Biol.* **1979**, *83*, 403–427.
- (7) Bloomfield, V. A. *Curr. Opin. Struct. Biol.* **1996**, *6*, 334–341.
- (8) Wilson, R. W.; Bloomfield, V. A. *Biopolymers* **1979**, *18*, 2192–2196.
- (9) Gosule, L. C.; Schellman, J. A. *Nature* **1976**, *259*, 333–335.
- (10) Widom, J.; Baldwin, R. L. *Biopolymers* **1983**, *2*, 1595–1620.
- (11) Mel'nikov, S. M.; Sergeev, V. G.; Yoshikawa, K. *J. Am. Chem. Soc.* **1995**, *117*, 2401–2408.
- (12) Laemmli, U. K. *Proc. Natl. Acad. Sci. U.S.A.* **1975**, *72*, 4288–4292.
- (13) Yoshikawa, K.; Takahashi, M.; Vasilevskaya, V. V.; Khokhlov, A. R. *Phys. Rev. Lett.* **1996**, *76*, 3029–3031.
- (14) Baigl, D.; Yoshikawa, K. *Biophys. J.* **2005**, *88*, 3486–3493.
- (15) Hud, N. V.; Downing, K. H. *Proc. Natl. Acad. Sci. U.S.A.* **2001**, *98*, 14925–14930.
- (16) Tsumoto, K.; Luckel, F.; Yoshikawa, K. *Biophys. Chem.* **2003**, *106*, 23–29.
- (17) Luckel, F.; Kubo, K.; Tsumoto, K.; Yoshikawa, K. *FEBS Lett.* **2003**, *579*, 5119–5122.
- (18) Niemeyer, C. M. *Angew. Chem., Int. Ed.* **2001**, *40*, 4128–4158.
- (19) Ganachaud, F.; Elaïssari, A.; Pichot, C.; Laayoun, A.; Cros, P. *Langmuir* **1997**, *13*, 701–707.
- (20) Sandström, P.; Boncheva, M.; Åkerman, B. *Langmuir* **2003**, *19*, 7535–7543.
- (21) Kneuer, C.; Sameti, M.; Bakowsky, U.; Schiestel, T.; Schirra, H.; Schmidt, H.; Lehr, C.-M. *Bionconjugate Chem.* **2000**, *11*, 926–932.
- (22) Radu, D. R.; Lai, C.-Y.; Jeftinija, K.; Rowe, E. W.; Jeftinija, S.; Lin, V. S.-Y. *J. Am. Chem. Soc.* **2004**, *126*, 13216–13217.
- (23) Zhu, J.; Tang, A.; Law, L. P.; Feng, M.; Ho, K. M.; Lee, D. K. L.; Harris, F. W.; Li, P. *Bionconjugate Chem.* **2005**, *16*, 139–146.
- (24) Cao, Y. C.; Jin, R.; Mirkin, C. A. *Science* **2002**, *297*, 1536–1540.
- (25) Mahtab, R.; Harden, H. H.; Murphy, C. J. *J. Am. Chem. Soc.* **2000**, *122*, 14–17.
- (26) Nakao, H.; Shiigi, H.; Yamamoto, Y.; Tokonami, S.; Nagaoka, T. Sugiyama, S.; Ohtani, T. *Nano Lett.* **2003**, *3*, 1391–1394.
- (27) Braun, E.; Eichen, Y.; Sivan, U.; Ben-Yoseph, G. *Nature* **1998**, *391*, 775–778.
- (28) Zinchenko, A. A.; Yoshikawa, K.; Baigl, D. *Adv. Mater.* **2005**, *17*, 2820–2823.
- (29) Kabanov, V. A.; Sergeev, V. G.; Pyshkina, O. A.; Zinchenko, A. A.; Zezin, A. B.; Joosten, J. G. H.; Brackman, J.; Yoshikawa, K. *Macromolecules* **2000**, *33*, 9587–9593.
- (30) Chen, W.; Turro, N. J.; Tomalia, D. A. *Langmuir* **2000**, *16*, 15–19.
- (31) Kukowska-Latallo, J. F.; Bielinska, A. U.; Johnson, J.; Spindler, R.; Tomalia, D. A.; Baker, J. R., Jr. *Proc. Natl. Acad. Sci. U.S.A.* **1996**, *93*, 4897–4902.
- (32) Tang, M. X.; Redemann, C. T.; Szoka, F. C., Jr. *Bionconjugate Chem.* **1996**, *7*, 703–714.
- (33) Keren, K.; Soen, Y.; Ben, Yoseph, G.; Gilad, R.; Braun, E.; Sivan, U.; Talmon, Y. *Phys. Rev. Lett.* **2002**, *89*, 088103.
- (34) Netz, R. R.; Joanny, J.-F. *Macromolecules* **1999**, *32*, 9026–9040.
- (35) Kunze, K.-K.; Netz, R. R. *Phys. Rev. Lett.* **2000**, *85*, 4389–4392.
- (36) Kunze, K.-K.; Netz, R. R. *Phys. Rev. E* **2002**, *66*, 011918.
- (37) Nguyen, T. T.; Shklovskii, B. I. *J. Chem. Phys.* **2001**, *115*, 7298–7308.
- (38) Grosberg, A. Yu.; Nguyen, T. T.; Shklovskii, B. I. *Rev. Mod. Phys.* **2002**, *74*, 329–345.
- (39) Schiessel, H.; Bruinsma, R. F.; Gelbart, W. M. *J. Chem. Phys.* **2001**, *115*, 7245–7252.
- (40) Schiessel, H. *J. Phys.: Condens. Matter* **2003**, *15*, 699–774.
- (41) Jonsson, M.; Linse, P. *J. Chem. Phys.* **2001**, *115*, 10975–10985.
- (42) Zinchenko, A. A.; Yoshikawa, K.; Baigl, D. *Phys. Rev. Lett.* **2005**, *95*, 228101.
- (43) Leuba, S. H.; Yang, G.; Robert, C.; Samori, B.; van Holde, K.; Zlatanova, J.; Bustamante, C. *Proc. Natl. Acad. Sci. U.S.A.* **1994**, *91*, 11621–11625.
- (44) Bednar, J.; Horowitz, R. A.; Dubochet, J.; Woodcock, C. L. *J. Cell Biol.* **1995**, *131*, 1365–1376.
- (45) Conwell, C. C.; Virfan, I. D.; Hud, N. V. *Proc. Natl. Acad. Sci. U.S.A.* **2003**, *100*, 9296–9301.
- (46) Grosberg, A. Yu.; Zhestkov, A. V. *J. Biomol. Struct. Dyn.* **1986**, *3*, 859–872.
- (47) Ubbink, J.; Odijk, T. *Europhys. Lett.* **1996**, *33*, 353–358.
- (48) Wang, G.; Murray, R. W. *Nano Lett.* **2004**, *4*, 95–101.
- (49) Dobrynin, A. V.; Rubinstein, M.; Obukhov, S. P. *Macromolecules* **1996**, *29*, 2974–2979.
- (50) Baigl, D.; Sferrazza, M.; Williams, C. E. *Europhys. Lett.* **2003**, *62*, 110–116.
- (51) Zinchenko, A. A.; Sergeev, V. G.; Murata, S.; Yoshikawa, K. *J. Am. Chem. Soc.* **2003**, *125*, 4414–4415.
- (52) Sakaue, T. *J. Chem. Phys.* **2004**, *120*, 6299–6305.
- (53) Miyazawa, N.; Sakaue, T.; Yoshikawa, K.; Zana, R. *J. Chem. Phys.* **2005**, *122*, 044902.
- (54) Sakaue, T.; Yoshikawa, K. *J. Chem. Phys.* **2006**, *125*, 074904.
- (55) Netz, R. R.; Andelman, D. *Phys. Rep.* **2003**, *380*, 1–95.
- (56) Schiessel, H.; Widom, J.; Bruinsma, R. F.; Gelbart, W. M. *Phys. Rev. Lett.* **2001**, *86*, 4414–4417.
- (57) Sakaue, T.; Yoshikawa, K.; Yoshimura, S. H.; Takeyasu, K. *Phys. Rev. Lett.* **2001**, *87*, 078105.
- (58) Chodanowski, P.; Stoll, S. *J. Chem. Phys.* **2001**, *115*, 4951–4960.
- (59) Wang, Y.; Kimura, K.; Huang, Q.; Dubin, P. L.; Jaeger, W. *Macromolecules* **1999**, *32*, 7128–7134.
- (60) Uberbacher, E. C.; Ramakrishnan, V.; Olins, D. E.; Bunick, G. J. *Biochemistry* **1983**, *22*, 4916–4923.
- (61) Yager, T. D.; McMurray, C. T.; van Holde, K. E. *Biochemistry* **1989**, *28*, 2271–2281.
- (62) Odijk, T. *J. Polym. Sci.* **1977**, *15*, 477–483.
- (63) Skolnick, J.; Fixman, M. *Macromolecules* **1977**, *10*, 944–948.
- (64) Podgornik, R.; Hansen, P. L.; Parsegian, V. A. *J. Chem. Phys.* **2000**, *113*, 9343–9350.
- (65) Baumann, C. G.; Smith, S. B.; Bloomfield, V. A.; Bustamante, C. *Proc. Natl. Acad. Sci. U.S.A.* **1997**, *94*, 6185–6190.
- (66) Wenner, J. R.; Williams, M. C.; Rouzina, I.; Bloomfield, V. A. *Biophys. J.* **2002**, *82*, 3160–3169.
- (67) Zinchenko, A. A.; Luckel, F.; Yoshikawa, K. *Biophys. J.* **2007**, *92*, 1318–1325.